Applied Catalysis B: Environmental 259 (2019) 118017

Contents lists available at ScienceDirect

Applied Catalysis B: Environmental

journal homepage: www.elsevier.com/locate/apcatb

A biomimetic nanoleaf electrocatalyst for robust oxygen evolution reaction

Bin Chen, Zhuo Zhang, Sangkuk Kim, Minki Baek, Dokyoung Kim, Kijung Yong*

Surface Chemistry Laboratory of Electronic Materials, Department of Chemical Engineering, Pohang University of Science and Technology (POSTECH), Pohang 37673, Republic of Korea

ARTICLE INFO

Keywords:
Biomimetic nanoleaf
Layered double hydroxide
Electrocatalysis
Oxygen evolution reaction
Water splitting

ABSTRACT

Oxygen evolution reaction (OER) is a key process in various advanced technologies for renewable energy conversion, such as water splitting and metal-air batteries. However, as a four-electron coupled reaction, the OER is kinetically sluggish and limited by its high overpotential and low efficiency. The design of novel nanostructured electrocatalysts is highly desirable to promote OER kinetics. Herein, a bio-inspired nanoleaf electrocatalyst has been successfully achieved for the first time by *in situ* growing ultrathin NiCo layered double hydroxide (LDH) nanosheets on CuO nanowires. Attributed to the mechanical support of CuO nanowire veins, the NiCo LDH lamina presents a large lateral size (more than 10 μm) and unique hierarchical structure that consisted of ultrathin nanosheets with numerous exposed edges. The CuO veins distributed across the LDH lamina can serve as the fast path for charge transfer and significantly promote the LDH conductivity. Compared to the conventional NiCo LDH nanosheets, the novel nanoleaves with enlarged electrochemical surface area, edge-rich active sites, and improved conductivity exhibit greatly enhanced OER performances with an impressive 9.3 fold enhanced activity, much lower overpotential of 262 mV at 10 mA cm^{-2}, as well as good stability and flexibility. The biomimetic nanoleaf structures and the corresponding design strategy can be broadly applied to other functional 2D materials for advanced applications.

1. Introduction

Due to rapid consumption of fossil fuels and associated environmental issues, the exploration and development of clean and sustainable energy sources have attracted increasing interests [1,2]. Among various advanced technologies for renewable energy conversion, electrochemical water splitting has emerged as a promising approach to produce environment-friendly hydrogen fuel from clean, renewable, but intermittent resources of energy [3–6]. However, the overall efficiency of electrochemical water splitting is seriously limited by the kinetically sluggish oxygen evolution reaction (OER) owing to its energetically unfavorable and four-electron reaction [7–10]. Therefore, the development of novel electrocatalysts is of great importance to promote OER kinetics and reduce the high overpotential required to drive OER process [11]. Currently, Ir/Ru-based noble metal oxides are recognized as the most active catalysts for OER; however, their commercial applications are unfortunately constrained by their high cost and scarcity, as well as catalytic instability [12–14].

Among the various electrocatalyst candidates for OER, first-row transition metal compounds have drawn great attention because of their earth abundance and easy availability [15–21]. Specifically, layered double hydroxides (LDHs)-based materials, a class of two-dimensional (2D) layered materials, have stood out from these effective catalyst candidates owing to their 2D structure and high theoretical activity [22–28]. However, the practical OER activity of LDHs is still far from the theoretical value due to their limited active sites and poor intrinsic conductivity. First, the synthetic LDHs usually consist of many closely stacked brucite-like layers and tend to form thick bulk bundles, which seriously limits the exposure of catalytically active surface area and edge sites [29]. Therefore, the bulk LDH particles need to be exfoliated into ultrathin nanosheets in various organic solvents to expose the hidden active sites [29–31]. To prepare electrodes for water splitting, the exfoliated ultrathin LDHs in the form of nanoparticle agglomerates need to be loaded onto conductive substrates such as glassy carbon and Ni foam by binder-assisted coating procedures, which easily leads to restacking of the as-exfoliated nanosheets and large electrical contact resistance between the catalysts and the supporting substrates [24,30]. To reduce the contact resistance, free-standing LDH nanosheets array can be directly grown on the conductive substrates [32–37]. Nevertheless, the as-grown LDHs generally possess a large thickness, leading to limited active surface area and OER activity. Therefore, the novel morphology design to increase the surface area and active sites is of essential significance for LDHs. In addition, another disadvantage of LDHs is their poor intrinsic electrical

* Corresponding author.
E-mail address: kyong@postech.ac.kr (K. Yong).

https://doi.org/10.1016/j.apcatb.2019.118017
Received 19 March 2019; Received in revised form 22 July 2019; Accepted 27 July 2019
Available online 02 August 2019

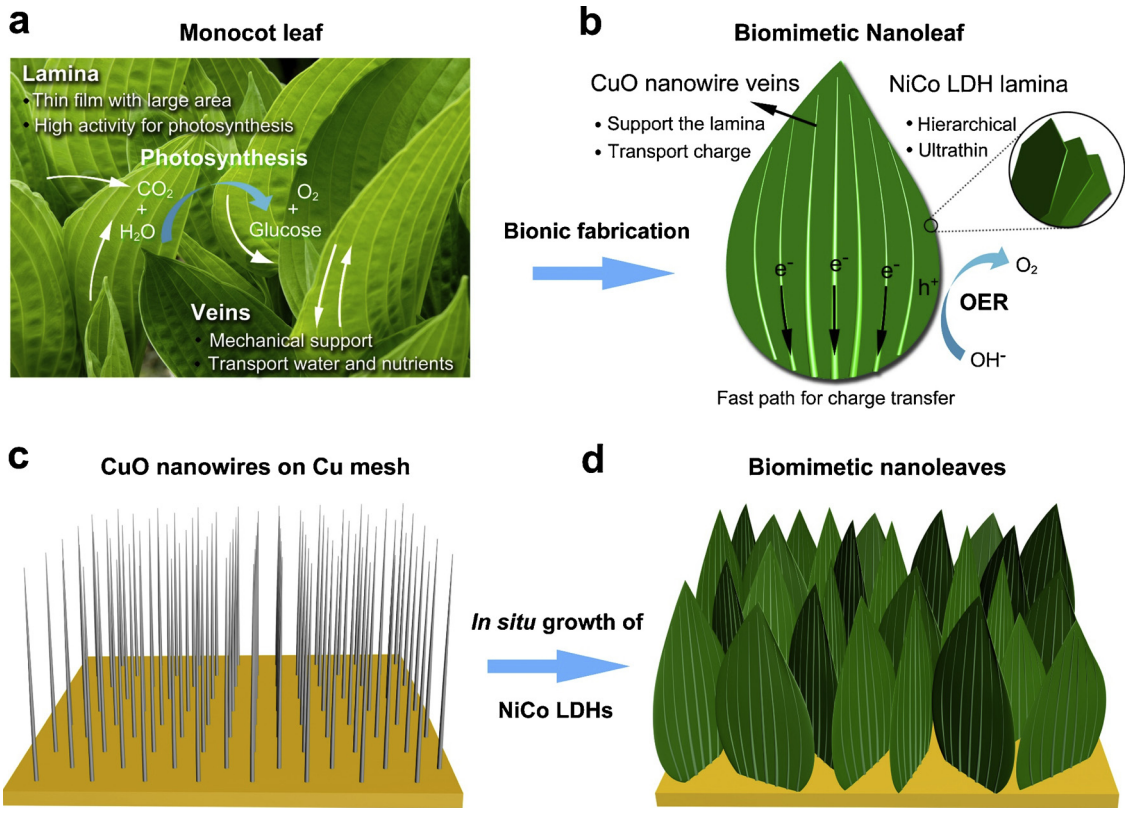

Fig. 1. Schematic illustration of the biomimetic nanoleaf electrocatalyst. (a) Photograph of the monocot leaf. (b) Biomimetic nanoleaf. (c, d) Schematic for the fabrication of biomimetic nanoleaves.

conductivity owing to the low intrinsic conductivity of metal hydroxides [24,29,36], with a relatively large band gap of 1.9~4.5 eV [38–41].To overcome this issue, the exfoliated LDHs have been integrated with conductive carbon materials, such as carbon nanotubes (CNTs) and reduced graphene oxide (RGO) [42–44]. These hybridized nanocomposites exhibited improved conductivity and OER activity; however, their long-term stability was unsatisfactory due to the corrosion of the carbon materials under harsh potential conditions [36,45]. Consequently, it is urgently desired to explore a novel strategy to synthesize ultrathin LDH nanosheets with enlarged active surface area and improved conductivity.

Herein, inspired by the leaf structure in nature, a biomimic nanoleaf was presented for the first time, which realized the efficient fabrication of ultrathin NiCo LDH nanosheets with large electrochemical surface area, numerous active edges, and improved conductivity. Similar to the leaf structure, the as-presented nanoleaves consisted of thin lamina and parallel veins, leading to a monocot leaf structure (Fig. 1a), which is different from the eudicot leaf with net pattern veins. CuO nanowires with a high density on a conductive Cu mesh were used as the veins to support the LDH nanosheet lamina and promote charge transfer, while the LDH lamina with a large surface area provided highly active sites for OER reaction (Fig. 1b). The biomimetic nanoleaf was fabricated by a combinatorial two-step process of synthesizing the CuO nanowire veins via annealing Cu mesh, and *in situ* growing the NiCo LDH thin lamina on the CuO veins by a hydrothermal method (Fig. 1c and d). Due to the mechanical support function of the CuO nanowires, the achieved NiCo LDH thin lamina exhibited a quite large surface area (more than 10 μm in lateral size). More interestingly, the large LDH laminar consisted of numerous ultrathin nanosheets (approximately 1.3 nm thick) with exposed active edge sites, leading to a hierarchical structure. The veins of CuO nanowires exhibited good conductivity and stability under the harsh potential conditions, and served as fast path for charge transfer to efficiently improve the LDH conductivity. As a result, the large electrochemical surface area, edge-rich, and ultrathin nanoleaves demonstrated robust OER performance with high catalytic activity and good long-term stability.

2. Experimental section

2.1. Materials

$Ni(NO_3)_2{\cdot}6H_2O$ (99.999%), $Co(NO_3)_2{\cdot}6H_2O$ (98%), *N,N-di*-methylformamide (DMF, 99.8%), and ethanol (99.5%) were purchased from Sigma-Aldrich Chemicals. All of the chemicals were used without further purification. Cu meshes were bought from the Alfa Aesar Corporation.

2.2. Synthesis of the biomimetic nanoleaf

The biomimetic nanoleaves were fabricated on a conductive Cu mesh by a combinatorial two-step process. First, Cu mesh was cut into small pieces (3 cm × 5 cm) and sequentially washed in ethanol. After annealing the Cu mesh at 500 °C in air for 5 h, CuO nanowires with high density were spontaneously grown on the Cu mesh [46,47]. Next, 0.25 mmol $Ni(NO_3)_2{\cdot}6H_2O$ was dissolved in a solution consisting of 15 mL DMF and 30 mL DI water, then 0.05 mmol $Co(NO_3)_3{\cdot}6H_2O$ was added and dissolved in the mixed solution. After vigorous stirring for 15 min, the precursor mixed solution was transferred into a 110 mL autoclave, and the CuO nanowires substrate was put into the solution. Finally, the autoclave sealed by stainless steel was heated at 120 °C for 14 h; following another heat treatment at 160 °C for 6 h. As a controlled experiment, CuO film was grown on Cu mesh by annealing Cu mesh at 500 °C in air for 2 h, and NiCo LDH nanosheets were synthesized on CuO film by the same hydrothermal conditions as mentioned above.

2.3. Characterization

The morphology and struture of the as-fabricated catalysts were investigated by field-emission scanning electron microscopy (FE-SEM, JEOL JSM-7800F Prime), high-resolution scanning transmission electron microscopy (HR-STEM, JEOL 2100F with Cs-corrector), and atomic force microscopy (AFM, Bruker Multimode 8). The structures of all the obtained samples were studied by X-ray diffraction (XRD, D/MAX-2500, Rigaku) with Cu Kα radiation and X-ray photoelectron spectroscope (XPS, ESCALAB 220i-XL) by using Mg Kα radiation. The mass loading of active NiCo LDH was measured by inductively coupled plasma-optical emission spectrometry (ICP-OES, Sprctro ARCOS).

2.4. Electrochemical measurements

Electrochemical measurements were performed in a three-electrode cell with Pt wire counter electrode and Hg/HgO reference electrode by using a electrochemical analyzer (model 263A, EG&G Princeton Applied Research) at room temperature. All the measurements were used 1.0 M KOH aqueous solution as the electrolytes. The potentials were calibrated to the reversible hydrogen electrode scale (E_{RHE}) by Nernst equation: $E_{RHE} = E_{Hg/HgO} + 0.059 \times pH + 0.098$. For Linear sweep voltammetry (LSV) polarization curves, the potentials were swept with a scan rate of 1 mV s^{-1}. All LSV curves were recorded after activating the catalysts by using cyclic voltammetry (CV) until reaching a stable state. To obtain the electrochemically active surface area (ECSA), CV was performed in a small potential range from 1.2 V to 1.3 V with various scan rates of 20, 40, 60, 80, 100, and 120 mV s^{-1}. Electrochemical impedance spectroscopy (EIS) was tested with overpotential bias of 300 mV in a frequency range from 0.1 Hz to 100 kHz. The long-term stability of the biomimetic nanoleaves was tested at 10 mA cm^{-2}. The produced H_2 and O_2 gases were measured and analyzed by using a gas chromatograph (GC 7890 B Series, Agilent) with a column (Mol Sieve 5A, SUPELCO) during stability test. The Faradaic efficiency for H_2 and O_2 gas production was estimated by comparing the experimentally measured gas volumes with their theoretical calculation values.

3. Results and discussion

3.1. Structure and morphology characterization

The structures of the biomimetic nanoleaf electrocatalysts were characterized by SEM. First, Fig. 2a shows that CuO nanowires with high density were vertically grown on Cu mesh. The surface of Cu was also oxidized to form a solid film that can promote the stability of Cu electrode during OER test [48]. The enlarged view shows that the average diameter of CuO nanowires was approximately 90 nm, while their length was from 15 to 45 μm (Fig. S1). The crystalline structure of CuO nanowires was studied by XRD. Fig. S2 shows that the Cu mesh was pure face centered cubic Cu (JCPDS Card No. 04-0836) [49–51]. After annealing the Cu mesh at 500 °C in air for 5 h, the Monoclinic CuO peaks with high intensity could be recognized (JCPDS Card No. 80-1917) [46,47,52]. Except for these peaks of CuO and Cu, other diffraction peaks belong to Cu_2O which originated from an interfacial Cu_2O layer between the CuO and Cu [46–48]. Then, the biomimetic nanoleaves were fabricated by *in situ* growing of NiCo LDH lamina on the CuO veins. The photographs show that the color of the sample changed from black to grayish, indicating that NiCo LDHs were deposited (Fig. S3). As shown in Fig. 2b, the as-synthesized nanoleaves were vertically arranged on the Cu mesh electrode, forming a highly dense and uniform nanoleaves array. The enlarged views reveal that the nanoleaf exhibited a unique structure similar as leaf in nature, which consisted of the CuO nanowire veins and the NiCo LDH lamina with a quite large lateral size over 10 μm (Fig. 2c and d). The corresponding EDS mapping analysis (Fig. S4) identifies the quintessential leaf-shaped structure, which clearly shows that Cu was in the vein part, while Ni, Co and O were homogeneously distributed throughout the whole LDH lamina. The close-up SEM image (Fig. 2d inset) shows the LDH lamina possessed a quite small thickness below 10 nm and consisted of many ultrathin nanosheets, thereby forming a hierarchical nanosheet structure. XRD was used to study the crystalline structure of the biomimetic nanoleaves. As shown in Fig. S2, the peaks of (003), (006), (012), (010) and (013) agreed well with the Ni-based LDH structure (JCPDS Card No. 38-0715) [32–35]. After peak fitting analysis, the interlayer distance of LDH could be calculated to be approximately 0.69 nm, which was corresponding to the reported LDHs [24,53]. The level of crystallization was estimated to be 35.2%. Except for these LDH peaks, all the other peaks of CuO nanowires, Cu mesh, and Cu_2O exhibited almost no changes, which demonstrated that the Cu nanowire substrate was stable during the fabrication of LDH lamina.

To reveal the leaf-shaped structure more clearly, the as-prepared nanoleaves without being destroyed were characterized *in situ* on Cu mesh by TEM. The NiCo LDH lamina and the CuO nanowire veins were clearly distinguished in the TEM image (Fig. 3a). The corresponding elemental mapping analysis (Fig. 3b-e) further confirms the CuO veins and NiCo LDH lamina forming the nanoleaf structure. Low-magnification TEM and the corresponding STEM mode were also carried out (Fig. S5). A high-angle annular dark field (HAADF)-STEM image reveals that the CuO nanowires acted as skeletons that strongly supported the whole LDH lamina. Moreover, the TEM images further identify that the hierarchical LDH lamina was composed of many ultrathin nanosheets. The enlarged TEM view shows the small nanosheets were nearly transparent to electron beams, indicating their ultrathin nature (Fig. 3f). The specific thickness of these lamina nanosheet was measured by AFM. As shown in the AFM images, several ultrathin nanosheets stacked together to form the lamina, and many nanopores could be seen on the single ultrathin nanosheets (Fig. 4a and Fig. S6a). The hierarchical layered structure was demonstrated more clearly in the 3D AFM image (Fig. S6b). The thickness of one ultrathin nanosheet was only approximately 1.3 nm, which was corresponding to two atomic layers of LDHs (Fig. 4b). While the heights of two and three ultrathin nanosheet layers were approximately 4.0 and 7.5 nm, respectively (Fig. 4c). The distances between two and three ultrathin nanosheet layers were much larger than the interlayer distances of NiCo LDHs (0.69 nm as calculated by XRD results), indicating that the hierarchical nanosheets of the LDH lamina were not closely-stacked, and there should be open space and gap between each hierarchical nanosheet.

As shown in the high-resolution TEM (HRTEM) image of the LDH lamina, the interplanar spacing of lattice fringe was recognized as 0.26 nm, agreeing well with the (012) plane of LDH (Fig. 3g) [32,35]. The corresponding selected area electron diffraction (SAED) patterns reveal well-defined rings, implying the polycrystalline nature of the NiCo LDH (Fig. 3g inset). The HRTEM image of the vein part identifies the fringe spacing as 0.25 nm, which was consistent with the ($\bar{1}$11) plane of CuO (Fig. 3h) [46,47]. The corresponding SAED patterns present well-defined patterns that demonstrate the high crystallinity of the CuO (Fig. 3h inset). XPS further demonstrated the existence of Ni, Co, Cu and O in the biomimetic nanoleaves (Fig. S7). As show in Fig. S7a, two Ni 2p spin-orbit doublets at binding energy (BE) of 855.8 eV and 873.6 eV, as well as their shakeup satellites could be recognized as the Ni $2p_{3/2}$ and Ni $2p_{1/2}$ signals [35,54]. After peak fitting analysis, the peaks can be separated to two distinct Ni species, which are attributed to Ni^{2+} of 855.5 eV and 872.8 eV, and Ni^{3+} at 856.6 eV and 873.9 eV according to the reported literatures [34,55]. The percentage of Ni^{3+} is approximately estimated to be 16.6%. The Co 2p XPS spectrum could be also fitted with two spin-orbit doublets, and the peaks of 782.1 eV and 797.1 eV are identified as Co^{2+}, and those of 780.7 eV and 795.7 eV are attributed to Co^{3+} with a content of 23.1% (Fig. S7b) [34,54–57]. In the Cu XPS spectrum (Fig. S7c), the peaks of 934.8 eV and 954.6 eV could be recognized as the Cu $2p_{3/2}$ and Cu $2p_{1/2}$ signals [48,58]. As shown in Fig. S7d, the O 1s spectrum can be fitted with two peaks,

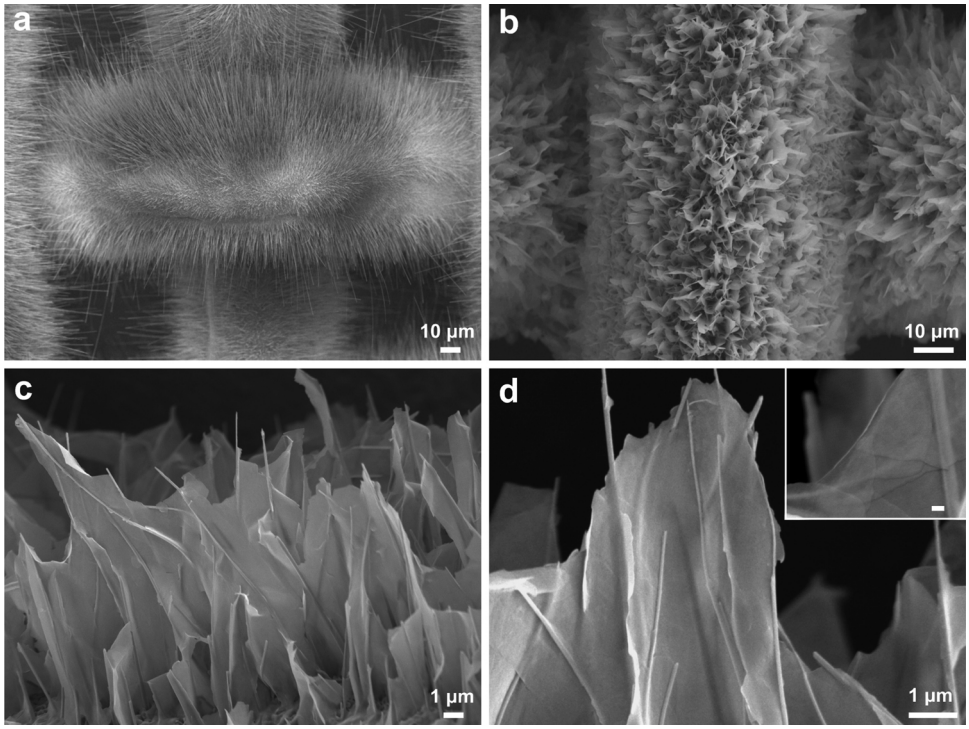

Fig. 2. SEM images of the obtained electrocatalysts. (a) CuO nanowires. (b–d) Biomimetic nanoleaves. Inset in (d): enlarged view of nanoleaves. Scale bar in the inset: 100 nm.

containing lattice oxygen (M–O, MN═i, Co and Cu) at BE of 529.4 eV and hydroxyl group (OH) at 531.3 eV [56,57,59]. The percentage of M–O is approximately estimated to be 9.8%.

It should be noted that the as-fabricated biomimetic nanoleaf presented a unique morphology compared to the previous LDH nanosheets directly grown on conductive substrates, such as Ni foam, carbon paper, Cu foil or mesh [32–37]. To reveal these morphology differences, NiCo LDH nanosheets with conventional morphology were grown on CuO/Cu mesh under the same hydrothermal conditions. First, a compact CuO film was grown on the Cu mesh by annealing in air in a shorter time (Fig. S8), then NiCo LDH nanosheets were arranged on the CuO film (Fig. S9). The average thickness of the NiCo nanosheets was about 20 nm, while the lateral sizes were about 2 μm in length and width, which shows similar morphology and sizes as the reported LDH nanosheets grown on the Ni foam or carbon paper [32–37]. The cross-sectional SEM images in Fig. S10 show that the height of the nanoleaves was achieved to more than 12 μm, which was much larger than that of the LDH nanosheets on CuO film (˜1.7 μm). Compared with the conventional LDH nanosheets, the presented biomimetic nanoleaf not only possessed a unique leaf-shaped morphology but also exhibited a greatly enlarged lateral size and reduced thickness. It can be inferred that the nanoleaves with hierarchical ultrathin nanosheets may possessed much larger surface area and more number of active edge sites.

3.2. Electrochemical performances for OER

Based on the above mentioned structural advantages, enhanced OER activity of the biomimetic nanoleaves was expected. The electrocatalytic OER performance of the prepared catalysts was investigated in a 1 M KOH electrolyte. Fig. 5a shows that the LSV curves of the biomimetic nanoleaves of NiCo LDHs supported by CuO nanowires, NiCo nanosheets on CuO film, CuO nanowires, and CuO film. First, the CuO nanowires presented a lower overpotential (423 mV) than that of the CuO film (442 mV) at a current density of 10 mA cm^{-2}. Interestingly, the biomimetic nanoleaves exhibited greatly promoted activity with a much lower overpotential of 262 mV than that of the conventional NiCo LDH nanosheets on CuO film (325 mV). The CuO nanowires on Cu mesh were used as the veins because the crystalline CuO shows a good conductivity and stability during the LDH growth and electrochemical testing [48]. At a quite low overpotential of 301 mV, the biomimetic nanoleaves revealed a high current density up to 50 mA cm^{-2}, which is 9.3 times as high as that of the conventional NiCo LDHs (5.39 mA cm^{-2}). To evaluate the kinetics of the OER, the corresponding Tafel slopes of the biomimetic nanoleaves and NiCo LDH nanosheets were obtained (Fig. 5b). The Tafel slope value of the nanoleaves was 49.36 mV dec^{-1}, which is much smaller than 83.92 mV dec^{-1} of the conventional NiCo LDH nanosheets. The lower Tafel slope value of the biomimetic nanoleaves demonstrated that the nanoleaf catalysts exhibit a faster OER rate, and more favorable electrocatalytic kinetics for OER. As Tafel slope is closely related to the electron and mass transport, the mechanism of promoted OER kinetics may be attributed to the unique hierarchical structure of biomimetic nanoleaf.

To further explore the mechanism of enhanced OER activity, ECSA and EIS measurements were carried out to estimate the electrochemical surface area and charge transfer kinetics, respectively. ECSA of the biomimetic nanoleaves and NiCo LDH nanosheets were evaluated from the electrochemical double-layer capacitance (C_{dl}). The C_{dl} value can be obtained by CV measurements under different scan rates to estimate the linear slope of the plot of capacitive current against scan rate [30]. The CV curves were tested with scan rates from 20 to 160 mV s^{-1} (Fig. S11). The plot of the current density difference against the scan rate was fitted to a linear regression (Fig. 5c). The biomimetic nanoleaves revealed a large slope value of 13.06 m F cm^{-2} that was approximately 3.79 times higher than the conventional NiCo LDH nanosheets (3.45 m F cm^{-2}), while the biomimetic nanoleaves achieved a 9.3 fold larger current density. The ICP measurements show that the mass loading of the active LDH for biomimetic nanoleaves was approximatel 0.6892 mg/cm^2, which was only 1.3 times higher than the conventional NiCo LDH nanosheets (0.5265 mg/cm^2), as shown in Table S1. The large electrochemical surface area of the biomimetic nanoleaves can be attributed to their hierarchical laminar structure with large lateral sizes and ultrathin thickness. To eliminate the influence of the active surface

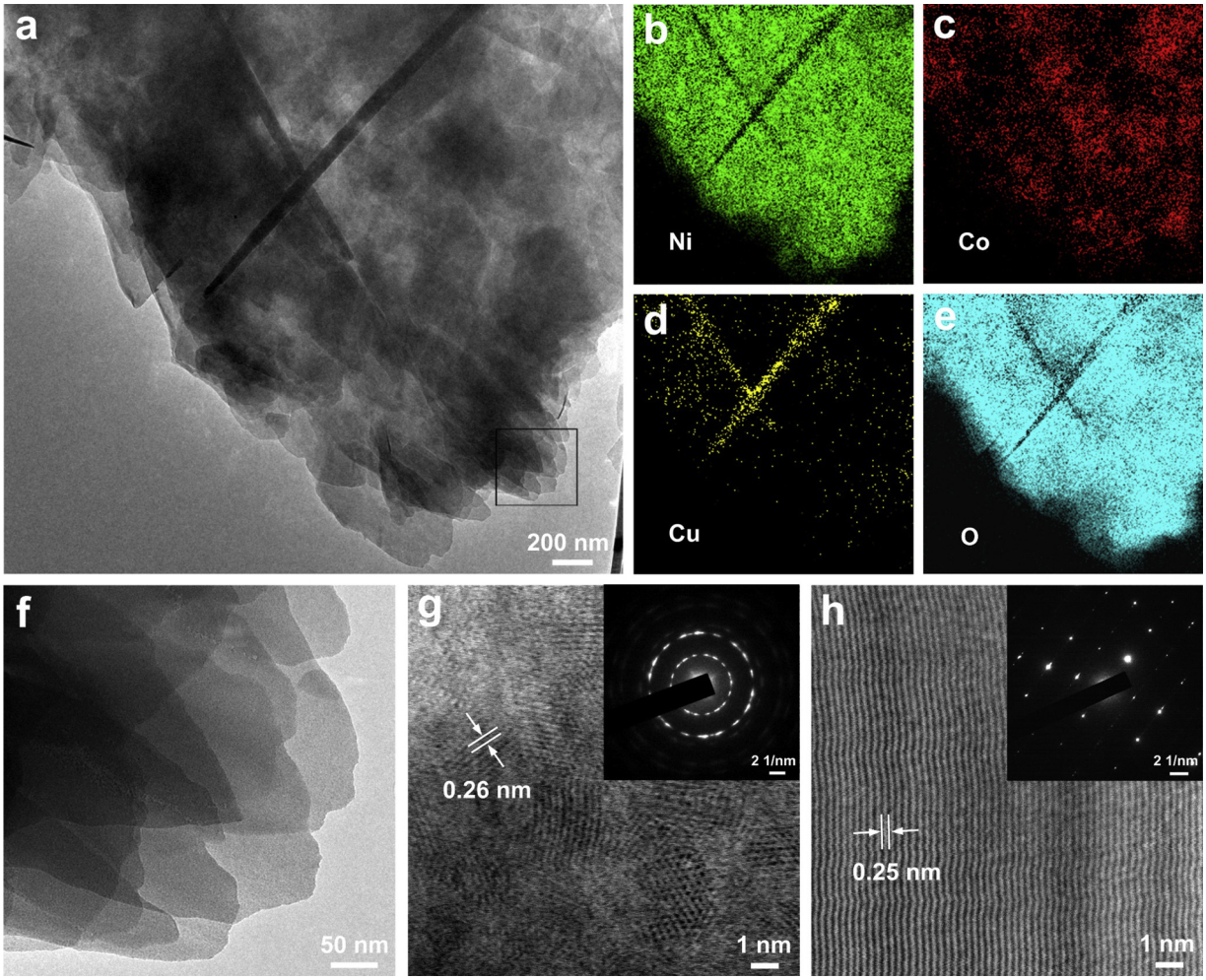

Fig. 3. TEM characterizations of biomimetic nanoleaves. (a) TEM image. (b–e) Corresponding elemental mapping images to reveal the distribution of Ni, Co, Cu, and O, respectively. (f) Enlarged views of the NiCo LDH laminar shown in (a). (g) HRTEM image of the NiCo LDH lamina. (h) HRTEM image of the CuO vein. Insets in (g) and (h) are the corresponding SAED patterns.

area and mass loading, LSV curves of the biomimetic nanoleaves and conventional NiCo nanosheets were normalized by using their relative ECSA and mass loading, respectively. As shown in Fig. S12, the nanoleaves still exhibited a higher OER activity than the NiCo nanosheets after ECSA and mass loading normalizing. These results demonstrated that the nanoleaves presented a much larger ECSA, which is a very important origin for the large improvement of OER activity, but not the only reason. It has been reported that the edges of the LDHs usually played an important role in OER process, and the edges could serve as the active sites and promoted OER kinetics [56,60,61]. In this regard, the hierarchical nanoleaf lamina consisted of many ultrathin nanosheets with numerous edges, leading to abundant active sites and further enhanced activity. The open space and gap between the hierarchical ultrathin nanosheets also favor the permeation of electrolyte to the active surface of LDHs. Additional reason for explaining enhanced OER activity of biomimetic nanoleaves comes from the improved conductivity by CuO nanowire veins. To prove this effect, EIS measurements were carried out for comparing the electrode kinetics of the biomimetic nanoleaves and conventional LDH nanosheets (Fig. 5d). The Nyquist plots of both catalysts show an apparent semicircle, and the

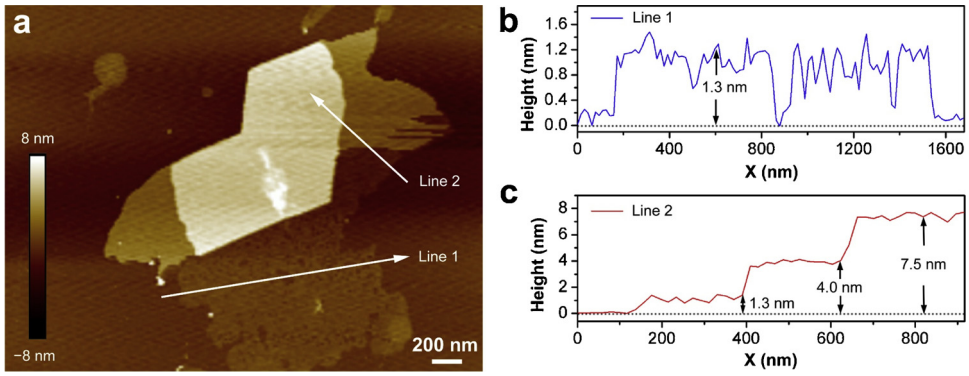

Fig. 4. AFM characterizations. (a) AFM image of the NiCo LDH lamina. (b, c) Corresponding height profiles of the NiCo LDH lamina across lines 1 and 2 in.(a).

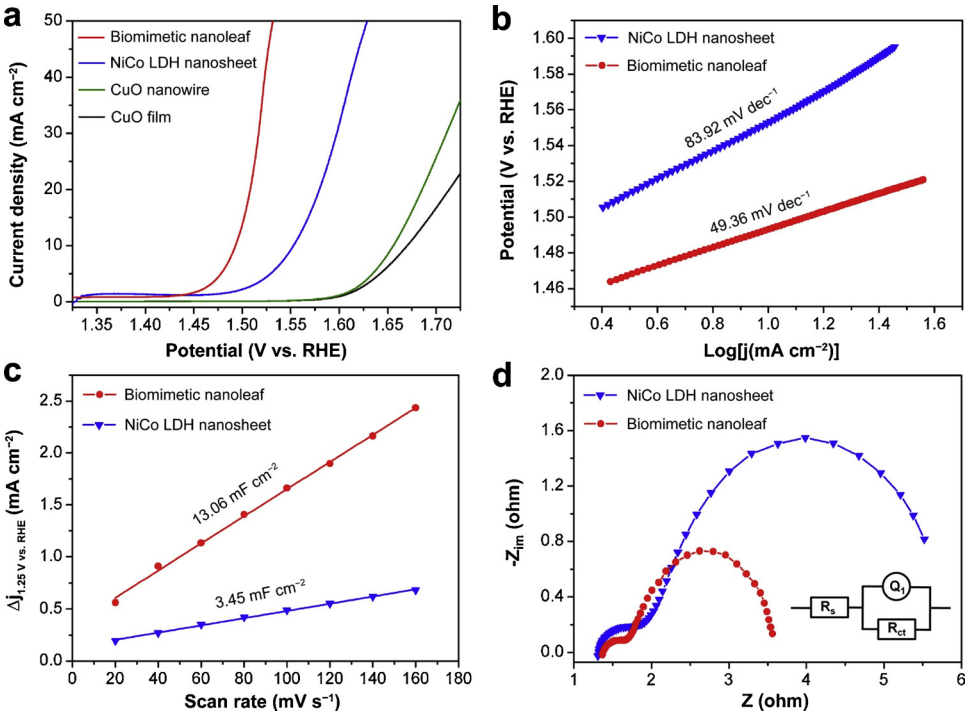

Fig. 5. OER performances. (a) LSV polarization curves of the CuO film, CuO nanowires, NiCo LDH nanosheets on CuO film, and biomimetic nanoleaves on CuO nanowires. (b) The corresponding Tafel plots of NiCo LDH nanosheets and biomimetic nanoleaves. (c) Capacitive current ($\Delta j = j_a - j_c$) plotted against the scan rates. (d) Nyquist plots at an overpotential of 300 mV in a frequency range from 0.1 Hz to 100 kHz.

diameter of the semicircle can be associated with the value of charge transfer resistance (R_{ct}) [22]. The nanoleaves showed a much smaller R_{ct} value (3.7 Ω) than that of the conventional NiCo LDHs (6.2 Ω). The small R_{ct} value indicates fast electron transport and catalytic kinetics, leading to a reduced Tafel slope. Thus, the nanoleaves exhibited an improved conductivity and catalytic kinetics, which agrees well with the low Tafel slope (Fig. 5b). This improved conductivity of the nanoleaves could be attributed to the plentiful CuO veins distributed across the whole LDH lamina. As reported, similar CuO@LDHs core@shell hybrid nanostructures have been studied and demonstrated as a good model for charge transport in the applications of supercapacitors and OER, the nanstrutured CuO with narrow band gap of 1.2˜1.7 eV and good conductivity could serve as the channels for electron transport [58,62–65]. Although this presented nanoleaves show a different morphology compared to the above-mentioned core@shell structures, the CuO nanowire veins have similar functions that not only support the thin LDH laminar, but also serve as the fast path for charge transfer, leading to a significantly reduced resistance of the LDHs and enhanced OER activity.

The electrochemical stability of the biomimetic nanoleaves was tested at a constant current density of 10 mA cm^{-2}. Fig. 6a inset shows the potential only increased 2.97% after more than 10 h of testing, revealing that the biomimetic nanoleaf electrocatalysts showed a good long-term stability. In addition, the produced H_2 and O_2 gas volumes were recorded at a steady-state current density of 5 mA cm^{-2} for 80 min (Fig. S13). As expected, the results show a linear relationship between the recorded gas volumes and water splitting time, and the ratio of measured H_2 and O_2 gas was about 2:1. The linear slopes could be calculated to be 0.5761 μL S^{-1} and 0.2863 μL S^{-1} for H_2 and O_2, which show a good agreement with the theoretically calculated values (0.5804 μL S^{-1} and 0.2902 μL S^{-1}). The Faradaic efficiency can be calculated to be nearly 100% for hydrogen and oxygen evolution. More interestingly, the biomimetic nanoleaves on Cu mesh exhibited a prominent flexibility. As shown in Fig. 6a, the LSV curves of the initial biomimetic nanoleaf electrode and sharp bending electrode demonstrated almost identical OER performances. The generated O_2 bubbles were homogeneously distributed through the whole sharp bending electrode, as shown in Fig. 6b. The O_2 bubbles could be seen more clearly in the video of the Supporting Information. This remarkable flexibility can be explained by the following reasons. First, the NiCo LDH thin lamina was strongly supported by the CuO nanowire veins, leading to a good structural integrity. Moreover, the nanoleaves were directly grown on the flexible Cu mesh, which effectively avoided the detachment during the electrochemical measurements as those

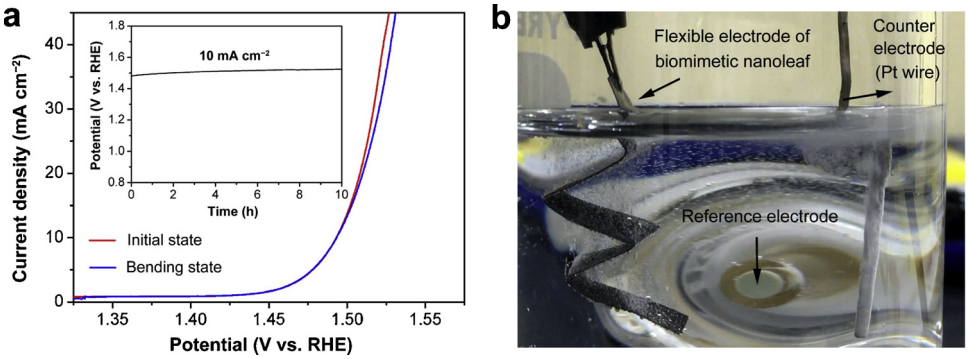

Fig. 6. Long-term stability and flexibility of the nanoleaf electrode. (a) LSV curves of the biomimetic nanoleaf electrode at initial and bending states. Insets in (a): Stability measurement at current density of 10 mA cm^{-2}. (b) Photograph of the nanoleaf electrode at bending state during the stability measurement at 20 mA cm^{-2}.

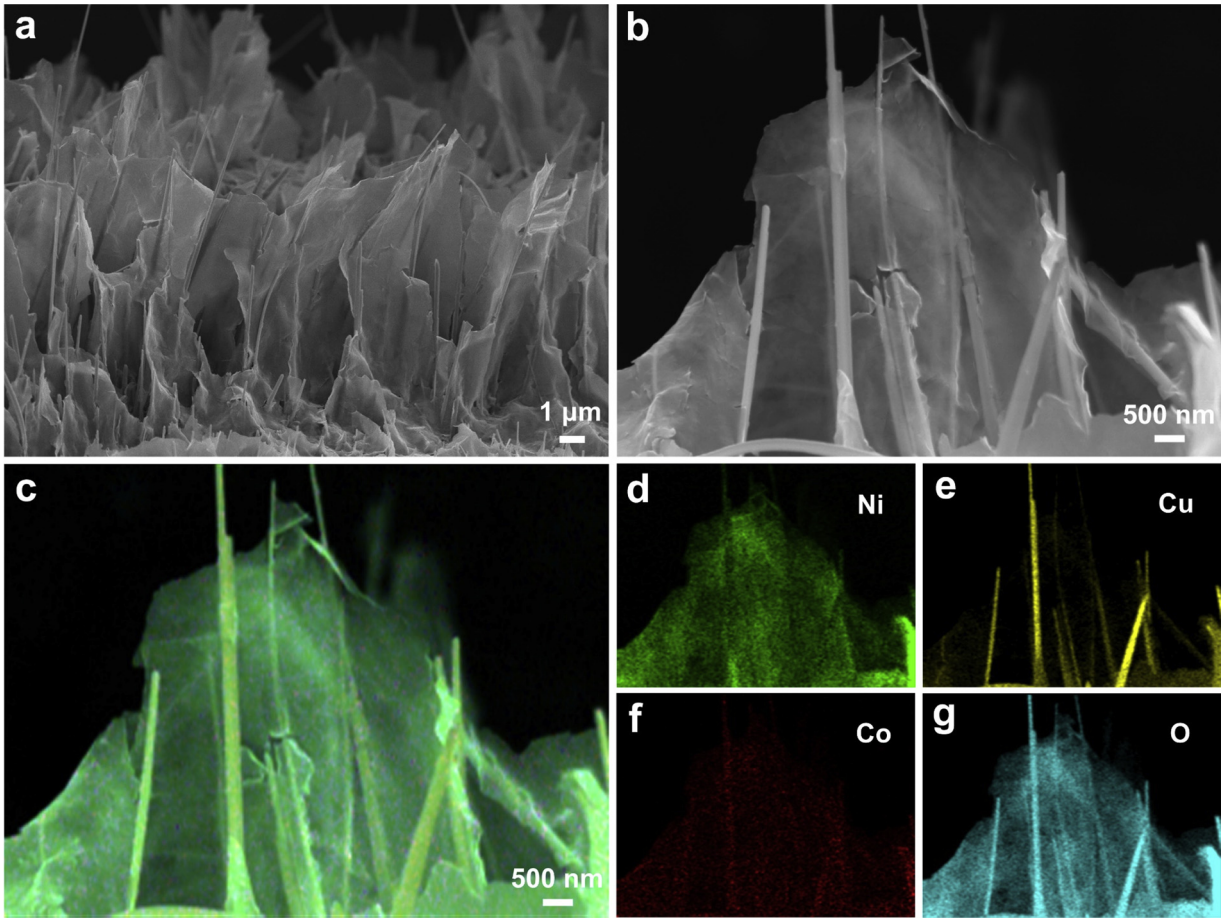

Fig. 7. SEM characterizations of biomimetic nanoleaves after long-term stability of OER. (a) SEM image. (b) Enlarged SEM view. (c) EDS layered image. (d–g) Corresponding elemental mapping images to reveal the distribution of Ni, Cu, Co, and O, respectively.

catalysts fixed on the electrode by binder-assisted coating method. These electrochemical results further highlight the superior OER performances of the biomimetic nanoleaf as a highly active, stable and flexible electrocatalyst. Compared with the recently reported electrocatalysts, the OER activity of the biomimetic nanoleaves is among the most active earth-abundant catalysts, even close to the Ir/Ru-based noble metal oxides (Table S2) [12–17,26,28,31–35,66–74].

After long-term OER stability test, the morphology and structure of the biomimetic nanoleaves were characterized by SEM, TEM, XRD, and XPS. SEM images show the presented electrocatalysts maintained their leaf-shaped morphology during the OER test (Fig. 7a). As shown in the enlarged SEM view, the nanoleaves exhibited no significant changes except for a little wrinkles and bending on the laminar edges (Fig. 7b). The corresponding EDS layered image and element mapping analysis show the elements of Ni, Co, Cu, and O had the similar distribution trend with the original nanoleaf (Fig. 7c–g). TEM images show that the hierarchical LDH lamina still consisted of many ultrathin nanosheets without damage, due to strong supporting function of the CuO nanowire veins (Fig. S14). XRD results demonstrate that the peaks of LDH and CuO exhibited no significant changes, and there was no new peak created after OER test, indicating that the main structures of LDH and CuO maintained (Fig. S15). As shown in Fig. S7, the Cu 2p XPS spectrum was very similar as that of the pristine nanoleaves, which further proved the CuO nanowire veins have a good stability during the OER test [48]. The peaks of Ni $2p_{3/2}$ and Ni $2p_{1/2}$ lightly shifted to the higher energy direction, and the content of Ni^{3+} increased from 16.6% to 26.7%, which demonstrated the Ni^{2+} was partially oxidized to Ni^{3+} during the OER test [33]. While the Co^{3+} and M–O contents also increased to 48.4% and 13.1%, indicating that the more catalytically active (oxy)hydroxide phase M–OOH (M = Ni and Co) formed on the surface of electrochemical catalysts at the beginning of OER test [57,59,75]. In general, the biomimetic nanoleaves maintained their original morphology in the OER test due to the supporting role of the CuO nanowire veins, and there was only a little wrinkle on the laminar edges. For the chemical structure, the main structure of the LDH laminar and CuO veins also maintained owing to their good stability, and only part of Ni^{2+} and Co^{2+} were oxidized to Ni^{3+} and Co^{3+} to form M–OOH on the surface during the OER test.

4. Conclusion

In conclusion, a novel biomimetic nanoleaf electrocatalyst consisting of NiCo LDH lamina and CuO nanowire vein has been successfully achieved by *in situ* growing LDH nanosheets on CuO nanowires. Compared with the previous LDH nanosheet structures, the biomimetic nanoleaves exhibited a unique morphology and much larger electrochemical surface area due to the strong supporting function of the CuO veins. The hierarchical NiCo LDH lamina was composed of many ultrathin nanosheets with numerous exposed active edge sites for OER. Moreover, the CuO nanowire veins acted as the fast path for charge transfer, which significantly promoted the LDH conductivity and facilitated the OER activity. As a result, the hierarchical biomimetic nanoleaves with enlarged surface area, edge-rich active sites, and improved conductivity demonstrated greatly enhanced OER performance with a quite small overpotential of 262 mV at 10 mA cm^{-2}, good stability and flexibility. The OER performance of the biomimetic nanoleaves can be further enhanced by optimizing the Ni and Co contents, and promoting the conductivity of CuO veins by using other conductive

and stable material. This biomimetic nanoleaf structure and design strategy can be broadly applied to other various 2D materials for advanced applications in electrochemical water splitting, photovoltaic cells, photoelectrochemical cells, supercapacitors, and electronic devices.

Declaration of Competing Interest

The authors declare that they have no known competing financial interests or personal relationships that could have appeared to influence the work reported in this paper.

Acknowledgement

This work was supported by the National Research Foundation of Korea (NRF-2019R1A2C2002156).

Appendix A. Supplementary data

Supplementary material related to this article can be found, in the online version, at doi:https://doi.org/10.1016/j.apcatb.2019.118017.

References

[1] S. Chu, A. Majumdar, Opportunities and challenges for a sustainable energy future, Nature 488 (2012) 294–303.
[2] J.S. Luo, J.H. Im, M.T. Mayer, M. Schreier, M.K. Nazeeruddin, N.G. Park, S.D. Tilley, H.J. Fan, M. Gratzel, Water photolysis at 12.3% efficiency via perovskite photovoltaics and Earth-abundant catalysts, Science 345 (2014) 1593–1596.
[3] J.F. Chang, Q. Lv, G.Q. Li, J.J. Ge, C.P. Liu, W. Xing, Core-shell structured $Ni_{12}P_5$/$Ni_3(PO_4)_2$ hollow spheres as difunctional and efficient electrocatalysts for overall water electrolysis, Appl. Catal. B: Environ. 204 (2017) 486–496.
[4] B. Chen, Z. Zhang, M. Baek, S. Kim, W. Kim, K. Yong, An antenna/spacer/reflector based Au/$BiVO_4$/WO_3/Au nanopatterned photoanode for plasmon-enhanced photoelectrochemical water splitting, Appl. Catal. B: Environ. 237 (2018) 763–771.
[5] S.H. Hsu, J.W. Miao, L.P. Zhang, J.J. Gao, H.M. Wang, H.B. Tao, S.F. Hung, A. Vasileff, S.Z. Qiao, B. Liu, An Earth-Abundant Catalyst-Based Seawater Photoelectrolysis System with 17.9% Solar-to-Hydrogen Efficiency, Adv. Mater. 30 (2018) 1707261.
[6] J.T. Zhang, Z.H. Zhao, Z.H. Xia, L.M. Dai, A metal-free bifunctional electrocatalyst for oxygen reduction and oxygen evolution reactions, Nat. Nanotechnol. 10 (2015) 444–452.
[7] J.Y. Liu, H. Xu, H.P. Li, Y.H. Song, J.J. Wu, Y.J. Gong, L. Xu, S.Q. Yuan, H.M. Li, P.M. Ajayan, In-situ formation of hierarchical 1D-3D hybridized carbon nanostructure supported nonnoble transition metals for efficient electrocatalysis of oxygen reaction, Appl. Catal. B: Environ. 243 (2019) 151–160.
[8] H. Sim, J. Lee, T. Yu, B. Lim, Manganese oxide with different composition and morphology as electrocatalyst for oxygen evolution reaction, Korean J. Chem. Eng. 35 (2018) 257–262.
[9] H. Shin, H. Xiao, W.A. Goddard, In Silico Discovery of New Dopants for Fe-Doped Ni Oxyhydroxide ($Ni_{1-x}Fe_xOOH$) Catalysts for Oxygen Evolution Reaction, J. Am. Chem. Soc. 140 (2018) 6745–6748.
[10] N.T. Suen, S.F. Hung, Q. Quan, N. Zhang, Y.J. Xu, H.M. Chen, Electrocatalysis for the oxygen evolution reaction: recent development and future perspectives, Chem. Soc. Rev. 46 (2017) 337–365.
[11] B. Zhang, X.L. Zheng, O. Voznyy, R. Comin, M. Bajdich, M. Garcia-Melchor, L.L. Han, J.X. Xu, M. Liu, L.R. Zheng, F.P.G. de Arquer, C.T. Dinh, F.J. Fan, M.J. Yuan, E. Yassitepe, N. Chen, T. Regier, P.F. Liu, Y.H. Li, P. De Luna, A. Janmohamed, H.L.L. Xin, H.G. Yang, A. Vojvodic, E.H. Sargent, Homogeneously dispersed multimetal oxygen-evolving catalysts, Science 352 (2016) 333–337.
[12] H. Hwang, T. Kwon, H.Y. Kim, J. Park, A. Oh, B. Kim, H. Baik, S.H. Joo, K. Lee, Ni@Ru and NiCo@Ru Core-Shell Hexagonal Nanosandwiches with a Compositionally Tunable Core and a Regioselectively Grown Shell, Small 14 (2018) 1702353.
[13] J. Lim, D. Park, S.S. Jeon, C.W. Roh, J. Choi, D. Yoon, M. Park, H. Jung, H. Lee, Ultrathin IrO_2Nanoneedles for Electrochemical Water Oxidation, Adv. Funct. Mater. 28 (2018) 1704796.
[14] L.C. Seitz, C.F. Dickens, K. Nishio, Y. Hikita, J. Montoya, A. Doyle, C. Kirk, A. Vojvodic, H.Y. Hwang, J.K. Norskov, T.F. Jaramillo, A highly active and stable IrO_x/$SrIrO_3$ catalyst for the oxygen evolution reaction, Science 353 (2016) 1011–1014.
[15] Y. Pan, K.A. Sun, S.J. Liu, X. Cao, K.L. Wu, W.C. Cheong, Z. Chen, Y. Wang, Y. Li, Y.Q. Liu, D.S. Wang, Q. Peng, C. Chen, Y.D. Li, Core-Shell ZIF-8@ZIF-67-Derived CoP Nanoparticle-Embedded N-Doped Carbon Nanotube Hollow Polyhedron for Efficient Overall Water Splitting, J. Am. Chem. Soc. 140 (2018) 2610–2618.
[16] S. Xue, L. Chen, Z.B. Liu, H.M. Cheng, W.C. Ren, $NiPS_3$Nanosheet-Graphene Composites as Highly Efficient Electrocatalysts for Oxygen Evolution Reaction, ACS Nano 12 (2018) 5297–5305.
[17] Y.F. Zhao, J.Q. Zhang, W.J. Wu, X. Guo, P. Xiong, H. Liu, G.X. Wang, Cobalt-doped MnO_2 ultrathin nanosheets with abundant oxygen vacancies supported on functionalized carbon nanofibers for efficient oxygen evolution, Nano Energy 54 (2018) 129–137.
[18] B.K. Kim, S.K. Kim, S.K. Cho, J.J. Kim, Enhanced catalytic activity of electrodeposited Ni-Cu-P toward oxygen evolution reaction, Appl. Catal. B: Environ. 237 (2018) 409–415.
[19] J.H. Kim, D.H. Youn, K. Kawashima, J. Lin, H. Lim, C.B. Mullins, An active nanoporous Ni(Fe) OER electrocatalyst via selective dissolution of Cd in alkaline media, Appl. Catal. B: Environ. 225 (2018) 1–7.
[20] Y.P. Liu, X. Liang, L. Gu, Y. Zhang, G.D. Li, X.X. Zou, J.S. Chen, Corrosion engineering towards efficient oxygen evolution electrodes with stable catalytic activity for over 6000 hours, Nat. Commun. 9 (2018) 2609.
[21] S. Wang, P. He, L.P. Jia, M.Q. He, T.H. Zhang, F.Q. Dong, M.Z. Liu, H.H. Liu, Y. Zhang, C.X. Li, J. Gao, L. Bian, Nanocoral-like composite of nickel selenide nanoparticles anchored on two-dimensional multi-layered graphitic carbon nitride: A highly efficient electrocatalyst for oxygen evolution reaction, Appl. Catal. B: Environ. 243 (2019) 463–469.
[22] K. Fan, H. Chen, Y.F. Ji, H. Huang, P.M. Claesson, Q. Daniel, B. Philippe, H. Rensmo, F.S. Li, Y. Luo, L.C. Sun, Nickel-vanadium monolayer double hydroxide for efficient electrochemical water oxidation, Nat. Commun. 7 (2016) 11981.
[23] A. Pirkarami, S. Rasouli, E. Ghasemi, 3-D CdS@NiCo layered double hydroxide core-shell photoelectrocatalyst used for efficient overall water splitting, Appl. Catal. B: Environ. 241 (2019) 28–40.
[24] Y.Y. Wang, D.F. Yan, S. El Hankari, Y.Q. Zou, S.Y. Wang, Recent Progress on Layered Double Hydroxides and Their Derivatives for Electrocatalytic Water Splitting, Adv. Sci. 5 (2018) 1800064.
[25] M. Xu, M. Wei, Layered double hydroxide-based catalysts: recent advances in preparation, structure, and applications, Adv. Funct. Mater. 28 (2018) 1802943.
[26] X. Xu, Z. Zhong, X.M. Yan, L.T. Kang, J.N. Yao, Cobalt layered double hydroxide nanosheets synthesized in water-methanol solution as oxygen evolution electrocatalysts, J. Mater. Chem. A 6 (2018) 5999–6006.
[27] Y.Q. Yang, W.B. Zhang, Y.L. Xiao, Z.P. Shi, X.M. Cao, Y. Tang, Q.S. Gao, $CoNiSe_2$ heteronanorods decorated with layered-double-hydroxides for efficient hydrogen evolution, Appl. Catal. B: Environ. 242 (2019) 132–139.
[28] L. Yu, J.F. Yang, B.Y. Guan, Y. Lu, X.W. Lou, Hierarchical hollow nanoprisms based on ultrathin Ni-Fe layered double hydroxide nanosheets with enhanced electrocatalytic activity towards oxygen evolution, Angew. Chem. Int. Ed. 57 (2018) 172–176.
[29] J.F. Yu, Q. Wang, D. O'Hare, L.Y. Sun, Preparation of two dimensional layered double hydroxide nanosheets and their applications, Chem. Soc. Rev. 46 (2017) 5950–5974.
[30] J.F. Ping, Y.X. Wang, Q.P. Lu, B. Chen, J.Z. Chen, Y. Huang, Q.L. Ma, C.L. Tan, J. Yang, X.H. Cao, Z.J. Wang, J. Wu, Y.B. Ying, H. Zhang, Self-assembly of single-layer CoAl-layered double hydroxide nanosheets on 3D graphene network used as highly efficient electrocatalyst for oxygen evolution reaction, Adv. Mater. 28 (2016) 7640–7645.
[31] F. Song, X.L. Hu, Exfoliation of layered double hydroxides for enhanced oxygen evolution catalysis, Nat. Commun. 5 (2014) 4477.
[32] B. Chen, Z. Zhang, S. Kim, S. Lee, J. Lee, W. Kim, K. Yong, Ostwald ripening driven exfoliation to ultrathin layered double hydroxides nanosheets for enhanced oxygen evolution reaction, ACS Appl. Mater. Interfaces 10 (2018) 44518–44526.
[33] H.F. Liang, F. Meng, M. Caban-Acevedo, L.S. Li, A. Forticaux, L.C. Xiu, Z.C. Wang, S. Jin, Hydrothermal continuous flow synthesis and exfoliation of NiCo layered double hydroxide nanosheets for enhanced oxygen evolution catalysis, Nano Lett. 15 (2015) 1421–1427.
[34] W.J. Liu, J. Bao, M.L. Guan, Y. Zhao, J.B. Lian, J.X. Qiu, L. Xu, Y.P. Huang, J. Qian, H.M. Li, Nickel-cobalt-layered double hydroxide nanosheet arrays on Ni foam as a bifunctional electrocatalyst for overall water splitting, Dalton Trans. 46 (2017) 8372–8376.
[35] C. Yu, Z.B. Liu, X.T. Han, H.W. Huang, C.T. Zhao, J. Yang, J.S. Qiu, NiCo-layered double hydroxides vertically assembled on carbon fiber papers as binder-free high-active electrocatalysts for water oxidation, Carbon 110 (2016) 1–7.
[36] J.L. Liu, Y. Zheng, Z.Y. Wang, Z.G. Lu, A. Vasileff, S.Z. Qiao, Free-standing single-crystalline NiFe-hydroxide nanoflake arrays: a self-activated and robust electrocatalyst for oxygen evolution, Chem. Commun. 54 (2018) 463–466.
[37] S.C. Sekhar, G. Nagaraju, J.S. Yu, Conductive silver nanowires-fenced carbon cloth fibers-supported layered double hydroxide nanosheets as a flexible and binder-free electrode for high-performance asymmetric supercapacitors, Nano Energy 36 (2017) 58–67.
[38] P.R. Chowdhury, K.G. Bhattacharyya, Ni/Co/Ti layered double hydroxide for highly efficient photocatalytic degradation of Rhodamine B and Acid Red G: a comparative study, Photochem. Photobiol. Sci. 16 (2017) 835–839.
[39] J. Guo, C.Y. Mao, R.K. Zhang, M.F. Shao, M. Wei, P.Y. Feng, Reduced titania@layered double hydroxide hybrid photoanodes for enhanced photoelectrochemical water oxidation, J. Mater. Chem. A 5 (2017) 11016–11025.
[40] X.J. Li, D.F. Du, Y. Zhang, W. Xing, Q.Z. Xue, Z.F. Yan, Layered double hydroxides toward high-performance supercapacitors, J. Mater. Chem. A 5 (2017) 15460–15485.
[41] Z.B. Liang, C. Qu, W.Y. Zhou, R. Zhao, H. Zhang, B.J. Zhu, W.H. Guo, W. Meng, Y.X. Wu, W. Aftab, Q. Wang, R.Q. Zou, Synergistic effect of Co-Ni hybrid phosphide nanocages for ultrahigh capacity fast energy storage, Adv. Sci. 6 (2019) 1802005.
[42] M. Gong, Y.G. Li, H.L. Wang, Y.Y. Liang, J.Z. Wu, J.G. Zhou, J. Wang, T. Regier, F. Wei, H.J. Dai, An advanced Ni-Fe layered double hydroxide electrocatalyst for water oxidation, J. Am. Chem. Soc. 135 (2013) 8452–8455.
[43] X. Long, J.K. Li, S. Xiao, K.Y. Yan, Z.L. Wang, H.N. Chen, S.H. Yang, A strongly coupled graphene and FeNi double hydroxide hybrid as an excellent electrocatalyst

for the oxygen evolution reaction, Angew. Chem. Int. Ed. 53 (2014) 7584–7588.
[44] S.M. Yin, W.G. Tu, Y. Sheng, Y.H. Du, M. Kraft, A. Borgna, R. Xu, A highly efficient oxygen evolution catalyst consisting of interconnected nickel-iron-layered double hydroxide and carbon nanodomains, Adv. Mater. 30 (2018) 1705106.
[45] I. Katsounaros, S. Cherevko, A.R. Zeradjanin, K.J.J. Mayrhofer, Oxygen electrochemistry as a cornerstone for sustainable energy conversion, Angew. Chem. Int. Ed. 53 (2014) 102–121.
[46] X.C. Jiang, T. Herricks, Y.N. Xia, CuO nanowires can be synthesized by heating copper substrates in air, Nano Lett. 2 (2002) 1333–1338.
[47] L. Aguilera, I. Montero, M.E. Davila, A. Ruiz, L. Galan, V. Nistor, D. Raboso, J. Palomares, F. Soria, CuO nanowires for inhibiting secondary electron emission, J. Phys. D Appl. Phys. 46 (2013) 165104.
[48] T.N. Huan, G. Rousse, S. Zanna, I.T. Lucas, X.Z. Xu, N. Menguy, V. Mougel, M. Fontecave, A dendritic nanostructured copper oxide electrocatalyst for the oxygen evolution reaction, Angew. Chem. Int. Ed. 56 (2017) 4792–4796.
[49] C.J. Huang, Q.W. Liu, W.J. Fan, X.Q. Qiu, Boron nitride encapsulated copper nanoparticles: a facile one-step synthesis and their effect on thermal decomposition of ammonium perchlorate, Sci. Rep. 5 (2015) 16736.
[50] C.P. Yu, W.C. Zhang, B. Hu, D.B. Ni, Zl. Zheng, J.P. Liu, K.F. Mai, W. Ren, Core/shell CuO/Al nanorod thermite film based on electrochemical anodization, Nanotechnology 29 (2018) 36LT02.
[51] L. Yu, H.Q. Zhou, J.Y. Sun, F. Qin, D. Luo, L.X. Xie, F. Yu, J.M. Bao, Y. Li, Y. Yu, S. Chen, Z.F. Ren, Hierarchical Cu@CoFe layered double hydroxide core-shell nanoarchitectures as bifunctional electrocatalysts for efficient overall water splitting, Nano Energy 41 (2017) 327–336.
[52] N.C.D. Nath, S.Y. Choi, H.W. Jeong, J.J. Lee, H. Park, Stand-alone photoconversion of carbon dioxide on copper oxide wire arrays powered by tungsten trioxide/dye-sensitized solar cell dual absorbers, Nano Energy 25 (2016) 51–59.
[53] N. Han, F.P. Zhao, Y.G. Li, Ultrathin nickel-iron layered double hydroxide nanosheets intercalated with molybdate anions for electrocatalytic water oxidation, J. Mater. Chem. A 3 (2015) 16348–16353.
[54] X.Q. Cai, X.P. Shen, L.B. Ma, Z.Y. Ji, C. Xu, A.H. Yuan, Solvothermal synthesis of NiCo-layered double hydroxide nanosheets decorated on RGO sheets for high performance supercapacitor, Chem. Eng. J. 268 (2015) 251–259.
[55] X.Y. He, R.M. Li, J.Y. Liu, Q. Liu, R.R. Chen, D.L. Song, J. Wang, Hierarchical $FeCo_2O_4$@NiCo layered double hydroxide core/shell nanowires for high performance flexible all-solid-state asymmetric supercapacitors, Chem. Eng. J. 334 (2018) 1573–1583.
[56] Y.Y. Wang, C. Xie, Z.Y. Zhang, D.D. Liu, R. Chen, S.Y. Wang, In situ exfoliated, N-doped, and edge-rich ultrathin layered double hydroxides nanosheets for oxygen evolution reaction, Adv. Funct. Mater. 28 (2018) 1703363.
[57] R. Liu, Y.Y. Wang, D.D. Liu, Y.Q. Zou, S.Y. Wang, Water-plasma-enabled exfoliation of ultrathin layered double hydroxide nanosheets with multivacancies for water oxidation, Adv. Mater. 29 (2017) 1701546.
[58] Y.Q. Guo, X.F. Hong, Y. Wang, Q. Li, J.S. Meng, R.T. Dai, X. Liu, L. He, L.Q. Mai, Multicomponent hierarchical Cu-Doped NiCo-LDH/CuO double arrays for ultralong-life hybrid fiber supercapacitor, Adv. Funct. Mater. 29 (2019) 1809004.
[59] X. Bo, Y.B. Li, R.K. Hocking, C. Zhao, NiFeCr hydroxide holey nanosheet as advanced electrocatalyst for water oxidation, ACS Appl. Mater. Interfaces 9 (2017) 41239–41245.
[60] C.L. Hu, L. Zhang, Z.J. Zhao, J. Luo, J. Shi, Z.Q. Huang, J.L. Gong, Edge sites with unsaturated coordination on core-shell Mn_3O_4@$Mn_xCo_{3-x}O_4$ nanostructures for electrocatalytic water oxidation, Adv. Mater. 29 (2017) 1701820.
[61] D.Q. Li, B.W. Ren, Q.Y. Jin, H. Cui, C.X. Wang, Nitrogen-doped, oxygen-functionalized, edge- and defect-rich vertically aligned graphene for highly enhanced oxygen evolution reaction, J. Mater. Chem. A 6 (2018) 2176–2183.
[62] X.M. Li, X. Du, X.L. Ma, Z.D. Wang, X.G. Hao, A. Abudula, A. Yoshida, G.Q. Guan, CuO nanowire@Co_3O_4 ultrathin nanosheet core-shell arrays: an effective catalyst for oxygen evolution reaction, Electrochim. Acta 250 (2017) 77–83.
[63] X.M. Li, G.Q. Guan, X. Du, J. Cao, X.G. Hao, X.L. Ma, A.D. Jagadale, A. Abudula, A sea anemone-like CuO/Co_3O_4 composite: an effective catalyst for electrochemical water splitting, Chem. Commun. 51 (2015) 15012–15014.
[64] Z.H. Li, M.F. Shao, L. Zhou, R.K. Zhang, C. Zhang, J.B. Han, M. Wei, D.G. Evans, X. Duan, A flexible all-solid-state micro-supercapacitor based on hierarchical CuO@layered double hydroxide core-shell nanoarrays, Nano Energy 20 (2016) 294–304.
[65] G.L. Liu, X. He, D. He, B.Y. Cui, L. Zhu, H. Suo, C. Zhao, Construction of CuO@Ni-Fe layered double hydroxide hierarchical core-shell nanorods arrays on copper foam for high-performance supercapacitors, J. Mater. Sci. - Mater. Electron. 30 (2019) 2080–2088.
[66] J.W. Nai, H.J. Yin, T.T. You, L.R. Zheng, J. Zhang, P.X. Wang, Z. Jin, Y. Tian, J.Z. Liu, Z.Y. Tang, L. Guo, Efficient electrocatalytic water oxidation by using amorphous Ni-Co double hydroxides nanocages, Adv. Energy Mater. 5 (2015) 1401880.
[67] L. Qian, Z.Y. Lu, T.H. Xu, X.C. Wu, Y. Tian, Y.P. Li, Z.Y. Huo, X.M. Sun, X. Duan, Trinary layered double hydroxides as high-performance bifunctional materials for oxygen electrocatalysis, Adv. Energy Mater. 5 (2015) 1500245.
[68] F. Song, X. Hu, Ultrathin cobalt-manganese layered double hydroxide is an efficient oxygen evolution catalyst, J. Am. Chem. Soc. 136 (2014) 16481–16484.
[69] Y.Y. Wang, Y.Q. Zhang, Z.J. Liu, C. Xie, S. Feng, D.D. Liu, M.F. Shao, S.Y. Wang, Layered double hydroxide nanosheets with multiple vacancies obtained by dry exfoliation as highly efficient oxygen evolution electrocatalysts, Angew. Chem. Int. Ed. 56 (2017) 5867–5871.
[70] Y. Gu, S. Chen, J. Ren, Y.A. Jia, C.M. Chen, S. Komarneni, D.J. Yang, X.D. Yao, Electronic structure tuning in Ni_3FeN/r-GO aerogel toward bifunctional electrocatalyst for overall water splitting, ACS Nano 12 (2018) 245–253.
[71] C.J. Li, B.W. Zhang, Y. Li, S.J. Hao, X. Cao, G. Yang, J.S. Wu, Y.Z. Huang, Self-assembled Cu-Ni bimetal oxide 3D in-plane epitaxial structures for highly efficient oxygen evolution reaction, Appl. Catal. B: Environ. 244 (2019) 56–62.
[72] F. Luo, Q. Zhang, X.X. Yu, S.L. Xiao, Y. Ling, H. Hu, L. Guo, Z.H. Yang, L. Huang, W.W. Cai, H.S. Cheng, Palladium phosphide as a stable and efficient electrocatalyst for overall water splitting, Angew. Chem. Int. Ed. 57 (2018) 14862–14867.
[73] H. Wu, X. Lu, G.F. Zheng, G.W. Ho, Topotactic engineering of ultrathin 2D non-layered nickel selenides for full water electrolysis, Adv. Energy Mater. 8 (2018) 1702704.
[74] X. Zhao, X.Q. Li, Y. Yan, Y.L. Xing, S.C. Lu, L.Y. Zhao, S.M. Zhou, Z.M. Peng, J. Zeng, Electrical and structural engineering of cobalt selenide nanosheets by Mn modulation for efficient oxygen evolution, Appl. Catal. B: Environ. 236 (2018) 569–575.
[75] J.F. Xie, X.D. Zhang, H. Zhang, J.J. Zhang, S. Li, R.X. Wang, B.C. Pan, Y. Xie, Intralayered ostwald ripening to ultrathin nanomesh catalyst with robust oxygen-evolving performance, Adv. Mater. 29 (2017) 1604765.